A comparative numerical study of cohesive and non-cohesive particles in a fluidized bed

Manogna Adepu

Department of Chemical and Biochemical Engineering, Rutgers, the State University of New Jersey, USA

Research Center Pharmaceutical Engineering GmbH, Inffeldg. 13/2, 8010 Graz, Austria

Under the guidance of

Dr. Rohit Ramachandran[+]

Dr. Khinast. J

+Corresponding author: Rohit Ramachandran, e-mail: rohit.r@rutgers.edu, Fax: +1 848-445-2581

Abstract:

Fully coupled CFD-DEM simulations were conducted to investigate the applicability of the van der Waals cohesive force model to a spray fluid bed. For the present simulation DEM was executed on the Graphic Unit Processing Unit (GPU) and the CFD on the Central Processing Unit (CPU). For this, DEM code XPS was coupled with CFD code AVL FIRE®. Based on this approach a bottom spray fluid bed coater was simulated for a process of 30 sec. The growth and breakage of agglomerates was numerically confirmed. Number of particles sprayed over the simulation time and mean velocity were monitored in both cohesive and non-cohesive systems to understand the behavior of fluidization.

List of contents

1. Introduction

Coating is a common unit operation in the pharmaceutical industry. The Coating layer may have different functions, from controlling release to taste masking [Cole 2002]. The oldest form of pharmaceutical coating is sugar coating. The coating liquid was applied by hand using ladles, where temperature and amount of drying air were critical. Due to difficulties in identification of product and high operator skills sugar coating lost its importance to film coating. Commonly, open bowl-shaped copper pans were used initially, where stainless steel is the material used today. In the beginning, 150-200 kg per batch was coated, which increased to 500-600 kg per batch with the use of newly improved coating pans such as Pelligrini pans (an angular pan that is rotated on a horizontal axis).

The first commercial film coated tablet was produced by Abbott in 1954 using a fluidized bed (Wurster) coating process with cellulose derivate. After 1975, due to increase in cost of organic solvents, strict regulations due to environmental concerns related to organic liquids, aqueous film coating became popular. With this trend towards aqueous film coating and vented coating pans, fluidized bed film coating is least used nowadays. Large pans having two vents (front and rear) with the drying air moving inside the coating drum are used today. A huge quality improvement was achieved after perforated pans were developed.

Coating has progressed through systematic research with its application in pharmaceutical industry. Different powders are used for making tablets and granules which are coated depending upon their application. Most of the powders are cohesive by nature, where few powders exhibit cohesive nature after getting wet when sprayed with liquid (coating). Experiments become complex in the handling and fluidization of these powders. This is due to the unpredictable behavior of the cohesive powders, which belong to group C of Geldart's classification [Geldart, 1973]. Such powders tend to form agglomerates of random massive size and shape due to interparticle forces. This effects the powder flow and flow properties, creating difficulties in understanding the fluidization process. In the case of cohesive powders, the interparticle forces are considerable and they control the behavior of a

bed composed of fine particles. Thus, during fluidization, the bed of powder cracks into large portions and the gas tends to flow into the gap between the fissures. Then, channeling occurs in the bed and, eventually, the gas-solid contact is very low and any heat and mass transfer operation is weakened. When particles are fluidized with air and where the distance between the particles are very small, there arises a particle-particle interaction forces. In most cases Vanderwaals forces are controlling compared to other interaction forces like, capillary and electrostatic forces. As this particle-particle interaction force is achieved by contact, no force is exerted between them, when the particles are not in contact. The force of interaction between two solids depends on the size, the shape of the particles and as well as the distance between the particles. These forces are calculated starting from the Derjaguin approximation [Derjaguin, 1934] and the theory of Lifshitz [Lifshitz, 1956]. The calculation of the Van der Waals forces is estimated as the sum of all interactions between molecules held on the surface of the particles. The magnitude of these forces increases with the size reduction of the particles and becomes dominating compared to the weight of the particles.

Owing to this unpredicted behavior of cohesive powders as a result of coating, it is important to understand the coating process handling cohesive powders in great detail. This work focuses on a comparative study between the cohesive and non-cohesive nature of a powder when subjected to coating. An additional cohesive force model was added to the existing model [Siegmann 2014] to simulate the cohesive powder. A large number of experimental work has been conducted to understand and optimize coating process for a consistent quality maintenance [brock 2012, Dubey 2012, mauritz 2010]. Some of the works deal with the cohesive powders [Turki 2008, Zhou 1999]. Computer simulations have established as a powerful tool to study this coating process. As simulations are conducted with experimental data, they are a complement to experiments. Although it does not give results matching reality due to model assumptions, they reduce the number of experiments. Many process parameters and interactions which are hard to measure experimentally can be measured using simulations. For example, to find out the terminal velocity of air pumped into a fluid bed, many experiments should be conducted which are

economical and time consuming. But one could simulate a fluid bed with varying air velocity just to find out the terminal velocity. This enables to perform lab scale experiments on a single desk-side Graphic Processing Unit (GPU) [jajcevic 2013].

In this work a two way coupling of Discrete Element Model (DEM) and Computational Fluid Dynamics (CFD) was used. The CFD-code solves the volume averaged Navier-Stokes equation to simulate the flow of continuum fluid in the gas phase. The DEM-code solves the Newton's second law of motion to simulate the motion of individual particles. Coupling between the CFD-code, AVL FIRE® and DEM-code XPS was established based on Compute United Device Architecture (CUDA) technology [Radeke et al. 2010]. Based on this a bottom spray fluid bed coater was simulated for a process time of 30 sec.

2. Simulation Methods

The complete work is concerned with the application of computer simulations on the investigation of coating processes. A detailed study of powder is conducted with two cases. One when it behaves as a cohesive powder and second when it behaves as a non-cohesive powder.

2.1. Discrete Element Model (DEM)

DEM is a first principle computational numerical technique with the theoretical basis of the method originating from Newton's laws of motion. The total force experienced by individual grains or particles in a granular system is modeled and the subsequent accelerations, velocities, and positions are tracked over a period of time. The total force is the summation of contact forces (particle/particle and particle/boundary), and body forces, such as gravity, fluid, magnetic, or electrostatic forces. The first DEM application for coating was proposed by Yamane et al. [Yamane 1995]. He used only 600 spherical tablets binding to computational limitations then. In recent times, DEM became a very valuable tool for bulk particle analysis in pharmaceutical industry [ketterhangen 2009b]. As the movement of particles in a coater is governed mostly by gravitational and inertial body forces in combination with particle-particle and particle-wall collisions, DEM is well suited to simulate coating of powders and

other similar particles like tablets. DEM captures the movement of individual particles such as velocity and position and saves it for a certain time span. Due to this, at any point the simulated time span is less than the total process duration. Generally, as in the present work, 3 sec of simulation takes 24 hours. So typically values are some minutes of simulated process versus a total duration of some hours.

One important concern with DEM is the shape of particles. In most of the cases, from literature, spherical particles are used which if not realistic. But it is known that particle shape is an important factor for numerical simulations [Abedi 2011]. Large scale realistic modeling is still beyond current computational capacity. However this might change in future with the increase in CPU power and advent of new approaches. DEM simulations are computationally expensive, and it is limited for a study of hundred thousand particles. In the current work, the in house DEM code XPS is used which is improved by newly available Compute United Device Architecture (CUDA) technology [Radeke 2010].

2.2. Computational Fluid Dynamics (CFD)

Fluid (gas and liquid) flows are governed by partial differential equations which represent conservation laws for the mass, momentum, and energy. Computational Fluid Dynamics (CFD) is the art of replacing such PDE systems by a set of algebraic equations which can be solved using digital computers. It gives an insight into flow patterns that are difficult, expensive or impossible to study using traditional (experimental) techniques. In simple terms, Computational Fluid Dynamics (CFD) is a method used to simulate the flow behavior of a liquid or a gas. Apart from the velocity field of a fluid, modern CFD software enables one to include different phases, considering heat and mass transfer between phases, or describe porous region. It is also possible to track the movement of particles in the flow (Euler-Lagrange approach). The particle movement is influenced by the flow of liquid in the system, which in turn is affected by particles (two way coupling). An approach involving the Euler-

Lagrange Discrete Droplet Method can be applied to simulate the spray flow in the surrounding air. In this approach the particles themselves can only have limited interactions (such as coalescing droplets), but no sophisticated models for particle collisions are included. For the full description of particle movement and collision in a fluid stream, a coupled DEM-CFD has to be applied. In present work CFD is executed on a Central Processing Unit (CPU) using the commercial CFD code AVL FIRE®.

2.3. CFD-DEM coupling

The interactions between the solid particles and fluid makes a platform to couple DEM and CFD. The approaches to couple them was developed giving the ability to consider air stream and particle movement and their interactions in a single simulation. This ability of CFD-DEM coupling makes it possible to simulate fluidic-granular systems. The main advantage of CFD-DEM is, it provides a detailed information on particle interactions, trajectories and forces acting on individual particles. With the increasing simulation capacity of DEM using GPU [Radeke 2010], the coupling of CFD-DEM has emerged as a high performance method for coupled CFD-DEM simulations with up to 9 million particles per GB of GPU-Memory. Also Kafui et al. (2011) showed maximal speed with 64 processing cores by applying a semi-automatic parallelization of CFD-DEM code.

The main objective of this work is to study the fluid flow patterns and understand the behavior of cohesive and non-cohesive powders using a new hybrid approach. The new CUDA technology was used for the particle simulation by coupling with an existing CFD-code. Data exchange between the two codes was done by AVL Code Coupling Interface (ACCI), which is a software component for co-simulations with an arbitrary number of instances of different simulation programs. This newly developed technology was validated by Jajcevic et al. (2013) using fluidized granular systems and was later used in the simulation of a wurster coater by Siegmann et al. (2014) [jajcevic, Eva].

Siegmann et al. (2014) has simulated a wurster coater by monitoring the residence time distribution and size distribution of the particles using the CFD-DEM model validated by Jajcevic et al. (2013). In the present work, same model has been used to simulate the non-cohesive powder. Additionally the Van der Waals cohesive force model has been introduced in the DEM-code to simulate the same powder (which is expected to behave as cohesive powder).

3. Theoretical background of CFD-DEM Model

The dispersed particle phase was treated as a collection on individual particles, whose movement is described by applying Newton's second law. Where the gas-phase dynamics was described by the incompressible Newtonian fluid based on an Euler approach. In simple terms, the model is an Euler-Lagrange approach for a non-reactive flow. The two phases, continuum and dispersed phases, are coupled via the momentum exchange between gas phase and particles.

In the following sections, the gas phase and the solid phase equations are explained followed by the particle-particle interactions and particle-wall interactions. Also, the Van der Waals cohesive force model added to the force models in Jajcevic et al. (2013) was introduced.

3.1 Gas-phase modeling

The gas phase is modeled by solving the volume-averaged Navier-Stokes equations. All the variable are considered to be locally volume-averaged quantities over the control volume V, which was chosen to be at least order of magnitude larger than the particle volume V_p. The conservation of mass leads to:

$$\frac{\partial}{\partial t}(\varepsilon f\, \rho f\,) + \nabla \cdot (\varepsilon f \rho f \mathbf{u} f) = 0, \tag{1}$$

where ρf is the fluid density, εf is the local volume fraction of the fluid, $\mathbf{u} f$ is the fluid velocity vector and t is the time. Similarly, the conservation of the momentum can be given as:

$$\frac{\partial}{\partial t}(\varepsilon f \, \rho f \boldsymbol{u}\mathfrak{f}) + \nabla \cdot (\varepsilon \mathfrak{f} \rho \mathfrak{f} \boldsymbol{u}\mathfrak{f} \boldsymbol{u}\mathfrak{f}) = -\varepsilon f \, \nabla p - \nabla \cdot (\varepsilon f \, \tau f) + \varepsilon f \, \rho f \boldsymbol{g} - \boldsymbol{S}p$$

(2)

where p is the hydrodynamic pressure, τf is the stress tensor, $\mathbf{g}$ is the gravitational acceleration and $\mathbf{S}p$ is the inter-phase momentum transfer source term between particles and fluid. The stress tensor is defined as

$$\tau = p\boldsymbol{I} + \sigma \tag{3}$$

where $\mathbf{I}$ is the unit matrix, and σ is the viscous stress tensor

$$\sigma = \mu f \, (\nabla \boldsymbol{u} f + \nabla \boldsymbol{u} f^T) - 2/3(\mu f \nabla . \boldsymbol{u} f \boldsymbol{I}) \tag{4}$$

with μf being the dynamic viscosity.

3.2 Solid-phase and drag phase modeling

The motion of each particle (considered a point source) is described by Newton's equation of motion

$$mp \, \frac{dup}{dt} = Vi\nabla p + \beta\left(\boldsymbol{u}_f - \boldsymbol{u}_p\right) + \sum Fpp + \sum Fpw + mp\boldsymbol{g} \tag{5}$$

where mp is the particle mass, $\mathbf{u}p$ is the particle velocity, $-Vi\nabla p$ is pressure gradient force, β is the inter-phase momentum transfer coefficient and the remaining terms are interaction forces between the interacting particles and walls and the gravity forces, respectively.

The angular momentum of the particle is calculated as

$$Ip\left(\frac{d\omega p}{dt}\right) = \sum \boldsymbol{Mp} \tag{6}$$

where ωp is particle angular velocity, Mp is the torque, and Ip it the moment of inertia.

The inter-phase momentum transfer coefficient was given as a function of the solid ε_s, and the fluid εf fractions, the particle Reynolds number Rep, the particle diameter dp and the particle density ρp. The model by [Gidaspow (1994)] combines the [Ergun (1952)] equation for dense regimes and a correlation proposed by Wen and Yu (1966) for more dilute regimes

$$\beta_{Ergun} = 150\left(\frac{\varepsilon s^2 \mu_f}{\varepsilon_f dp^2}\right) + 1.75\left(\frac{\varepsilon s \rho_f}{dp}\right)|\boldsymbol{u}_f - \boldsymbol{u}_p| \qquad \text{for } \varepsilon<0{:}8,$$

$$\beta_{Wen-Yu} = \left(\frac{3}{4}\right)C_D\left(\frac{\varepsilon s \rho_f}{dp}\right)|\boldsymbol{u}_f - \boldsymbol{u}_p|\varepsilon_f^{-2.65} \qquad \text{for } \varepsilon<0{:}8, \tag{7}$$

where the drag coefficient C_D and the particle Reynolds number Rep are expressed as

$$C_D = \begin{cases} \frac{24}{\varepsilon_f Re_p}\left[1 + 0.15\left(\varepsilon_f Re_p\right)^{0.687}\right] & Re_p < 1000 \\ 0.44 & Re_p \geq 1000 \end{cases}$$

(8)

$$Re_p = \frac{\rho_f|\boldsymbol{u}_f - \boldsymbol{u}_p|d_p}{\mu_f} \tag{9}$$

To avoid the discontinuity between the two equations, Huilin and [Gidaspow (2003)] introduced an additional function that describes the transition between the regimes

$$\varphi_{gs} = \frac{arctan[150 \times 1.75(0.2 - \varepsilon_s)]}{\pi} + 0.5 \tag{10}$$

Using Eq. (10) the inter-phase momentum transfer coefficient can be calculated as

$$\beta = (1 - \varphi_{gs})\beta_{Ergun} + \varphi_{gs}\beta_{Wen-Yu} \tag{11}$$

By applying Lattice–Boltzmann simulations, [Koch and Hill (2001)] determined the inter-phase momentum transfer coefficient:

$$\beta = \frac{18\mu_f \varepsilon_f^2 \varepsilon_p}{d_p^2}\left(F_0(\varepsilon_p) + \frac{1}{2}F_3 \varepsilon_f Re_p\right)\frac{V_p}{\varepsilon_p}, \tag{12}$$

The particle Reynolds number $Re_p{}'$ is calculated taking into account the fluid volume fraction

$$Re_p{}' = \frac{\varepsilon_f \rho_f |\boldsymbol{u}_f - \boldsymbol{u}_p| d_p}{\mu_f} \tag{13}$$

In Eq. (12)

$$F_0(\varepsilon_p) = \begin{cases} \dfrac{1 + 3\sqrt{\varepsilon_p/2} + 2.109\varepsilon_p \ln(\varepsilon_p) + 16.14\varepsilon_p}{1 + 0.681\varepsilon_p - 8.48\varepsilon_p{}^2 + 8.14\varepsilon_p{}^3} & if \quad \varepsilon_p < 0.4 \\ \dfrac{10\varepsilon_p}{\varepsilon_f{}^3} & if \quad \varepsilon_p \geq 0.4 \end{cases} \tag{14}$$

$$F_3(\varepsilon_p) = 0.0673 + 0.212\varepsilon_p + \frac{0.0232}{\varepsilon_f^5} \tag{15}$$

From the most recently proposed model by [jajcevic 2013], which was used by [Pepiot and Desjardins (2012)], the inter-phase momentum transfer coefficient of the model is as follows:

$$\beta = \frac{18\mu_f \varepsilon_f}{\rho_p d_p^2} F(\varepsilon_f, Re_p) m_p \tag{16}$$

where F(ε_f, Re$_p$)m$_p$ is the dimensionless drag force coefficient proposed by [Beetstra et al. (2007a)], given as

$$F(\varepsilon_f, Re_p) = 10\frac{1-\varepsilon_f}{\varepsilon_f^2} + \varepsilon_f^2(1 + 1.5\sqrt{1-\varepsilon_f})$$

$$+ \frac{0.413 Re_p}{24\varepsilon_f^2}\left(\frac{\varepsilon_f^{-1} + 3\varepsilon_f(1-\varepsilon_f) + 8.4Re_p^{-0.343}}{1 + 10^{3(1-\varepsilon_f)}P\varepsilon_p^{-0.5-2(1-\varepsilon_f)}}\right)$$

(17)

where the particle Reynolds number is calculated taking into account the fluid volume fraction εf as given in Eq. (13).

The models described above were developed based on experimental data and was validated by [Jajecieve 2013]. He investigated whether the models correctly predicted the pressure drop in a fixed mono disperse particle bed.

3.3 Particle-particle and particle-wall interactions modeling

Since fluidized beds operate near the close-packing limit, particle–particle collisions are frequent and dominate the process. Thus, describing particle–particle interactions is critical to predicting the bed's dynamics.
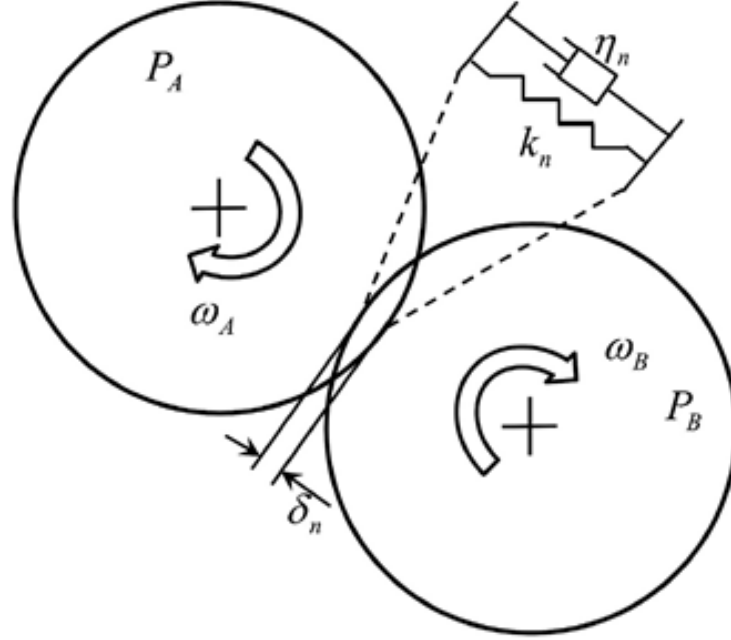
Fig. 1. Soft-sphere model of a particle-particle interaction.

There are several ways of describing particle–particle interactions. i.e., via volumetric, hard and soft-sphere models. In this work the soft-sphere approach (Fig. 1) model was used in this, where a linear-spring and dashpot model is employed to calculate the contact forces. When two particles are in contact with each other (see Fig. 1), a slightly overlap δn occurs resulting in a repulsive force. The force's magnitude depends on the overlap between the two particles, their relative velocity, the spring stiffness and the damping parameter, according to

$$F_{p_A \rightarrow p_B, n} = -k_n \delta_n \boldsymbol{n}_{AB} - \eta_n \boldsymbol{u}_{AB,n},$$

(18)

where k_n is the spring stiffness, $u_{AB,\,n}$ is the normal relative velocity vector of particles A and B, n_{AB} is the unit vector between the center of particle B and A, and η_n is the damping parameter expressed as

$$\eta_n = -2\ln(e_{n,p\to p})\frac{\sqrt{m_{AB}k_n}}{\sqrt{\pi^2 + (ln(e_{n,p\to p}))^2}}$$

With, (19)

$$m_{AB} = \left(\frac{1}{m_A} + \frac{1}{m_B}\right)^{-1}$$

In this expression, $0 < e_{n,p\text{-}p} < 1$ is the normal coefficient of restitution, and mA, mB are the masses of particles A and B, respectively.

The relative velocity vector is calculated as follows:

$$\boldsymbol{u}_{AB} = \boldsymbol{u}_A - \boldsymbol{u}_B - (R_A\omega_A + R_B\omega_B) \times \boldsymbol{n}_{AB}$$

(20)

and the normal relative velocity as

$$\boldsymbol{u}_{AB,n} = (\boldsymbol{u}_{AB}.\boldsymbol{n}_{AB})\boldsymbol{n}_{AB}$$

(21)

The unit vector between the center of particle A and B is given by

$$n_{AB} = \frac{\boldsymbol{P}_B - \boldsymbol{P}_A}{|\boldsymbol{P}_B - \boldsymbol{P}_A|},$$

(22)

Where **p** presents the position vector of particle.

For the tangential component of the contact force a Coulomb-type friction law is used (see Deen et al., 2007):

$$\boldsymbol{F}_{p_A\to p_B,t} = \begin{cases} -k_t\boldsymbol{\delta}_t - \eta_t\boldsymbol{u}_{AB,t} & if \ \left|\mathbf{F}_{P_A\to p_B,t}\right| \le \left|\mathbf{F}_{P_A\to p_B,n}\right| \\ -\mu_{fr,p\to p}\left|\mathbf{F}_{P_A\to p_B,n}\right|t_{AB} & if \ \left|\mathbf{F}_{P_A\to p_B,t}\right| > \left|\mathbf{F}_{P_A\to p_B,n}\right| \end{cases}$$

(23)

where k_t, δ_t, η_t, $\mu_{fr,p\text{-}p}$ and t_{AB} are the tangential spring stiffness tangential displacement, tangential damping coefficient, friction coefficient, and tangential unit vector, respectively.

The tangential displacement is given as

$$\delta_t = \boldsymbol{u}_{AB,t} . \Delta t \tag{24}$$

The tangential velocity $u_{AB,t}$ can be calculated as follows:

$$\boldsymbol{u}_{AB,t} = \boldsymbol{u}_{AB} - \boldsymbol{u}_{AB,n} \tag{25}$$

The tangential damping coefficient is expressed as follows:

$$\eta_t = -2\ln(e_{t,p \to p}) \frac{\sqrt{(2/7)m_{AB}k_t}}{\sqrt{\pi^2 + (ln(e_{t,p \to p}))^2}} \tag{26}$$

In this expression, $0 < e_{t,p \to p} < 1$ is the tangential coefficient of restitution. The tangential unit vector is calculated using the tangential velocity,

$$\boldsymbol{t}_{AB} = \frac{\boldsymbol{u}_{AB,t}}{|\boldsymbol{u}_{AB,t}|} \tag{27}$$

The particle–wall collision is handled by treating the walls as particles with an infinite mass, a zero radius (ie., $m_{AB} = m_A$), and a zero angular velocity. In Eq. (23), the tangential force at the wall is calculated using the wall friction coefficient $\mu_{fr,p\text{-}w}$ between the interacting particle and the wall.

For implementing cohesion between particles the additional cohesive force $F_{va,}$ was introduced. For dry particles, the cohesive force between two agglomerates is predominantly the van der Waals force. According to

Israelachvili's theory of intermolecular and surface forces , the van der Waals force between two spherical agglomerates of diameter d_{a1} and d_{a2} is given as,

$$F_{va} \approx \frac{A}{12\delta^2} \frac{d_{a1}d_{a2}}{d_{a1}+d_{a2}} \tag{28}$$

where δ is the distance between two particles, d_{a1} and d_{a2} are the diameter of particles and A is Hamaker constant, taken as 10^{-19} J.

3.4 Particle-coating modeling

The spray nozzle is modeled by defining a conical spray zone located inside the fluid bed on the bottom. In the spray nozzle, which is assumed to be a single point, many rays originate. The size of the resulting spray zone depends on the opening angle of the cone. Each of the rays detects intersecting particles. Particles hit by these rays increase their radii according to their residence time in the spray zone. The spraying is done in every single DEM-timestep.

3.5 CFD-DEM model

The gas and the solid phases are coupled via the source term $\mathbf{S}p$ and the gas volume fraction ε_f (Eqs. (1) and (2)). To avoid the issue in the time-consuming data exchange between the CPU-based CFD-code and the GPU-based DEM-code, the amount of data exchanged must be kept to a minimum in order to minimize the global communication overhead. In Fig. 2, the scheme of the coupling between the CFD-code AVL FIRE and the DEM-code XPS is shown, which is adapted from [Jajcevic et al (2013)].
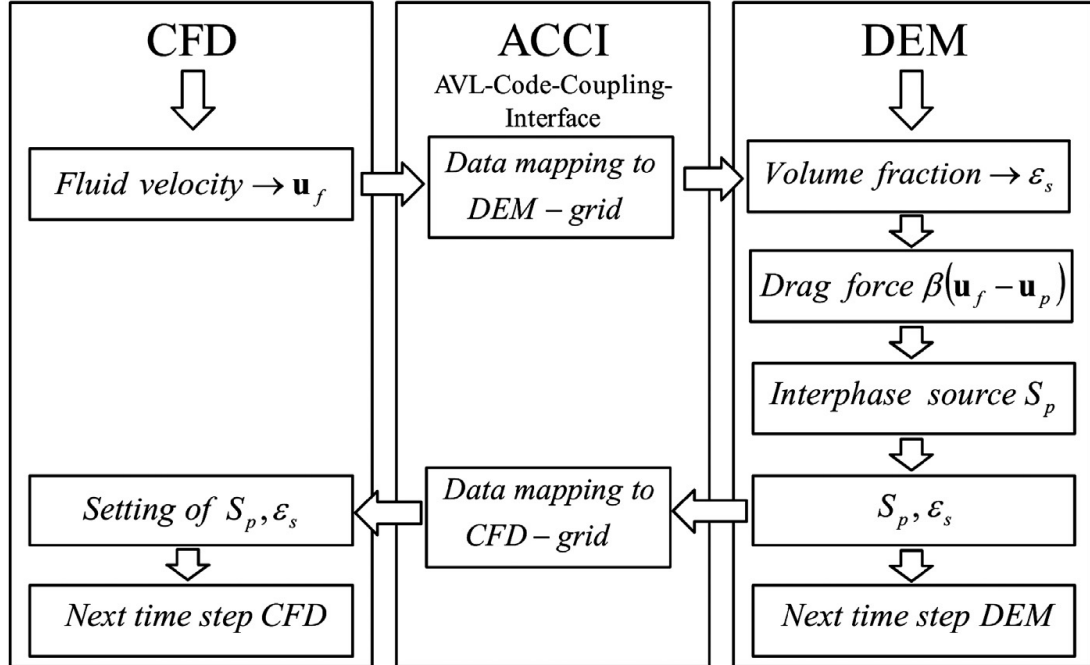
CFD	ACCI	DEM
⇩	AVL-Code-Coupling-Interface	⇩
Fluid velocity $\rightarrow \mathbf{u}_f$	*Data mapping to DEM – grid*	*Volume fraction* $\rightarrow \varepsilon_s$
		Drag force $\beta\left(\mathbf{u}_f - \mathbf{u}_p\right)$
		Interphase source S_p
Setting of S_p, ε_s	*Data mapping to CFD – grid*	S_p, ε_s
Next time step CFD		*Next time step DEM*

Fig. 2. Scheme of the CFD–DEM coupling method.

First the fluid velocity field is transferred via ACCI to the DEM code residing in the GPU memory. Following that, the DEM code calculates the drag force acting on each particle on the GPU. Then, the resulting force field from the particle phase is transferred back to the CFD code by the ACCI link. With this algorithm a first-order temporal accuracy can be achieved. Due to the small size of the time steps required by the DEM code for resolving particle collisions, the temporal errors are likely to be insignificant.

The algorithm involves a non-trivial mapping between a given, arbitrary shaped CFD mesh and the regular DEM grid which is present for the linearization of the particle neighbor search. The CFD mesh is generated via an automated grid generation algorithm, resulting in an irregular spatial subdivision of the simulation volume. This mesh can be very different in size, resolution and morphology from the DEM grid, which is formed by simple cubes. The mapping algorithm realizes both, the interpolation of the fluid velocity vectors, to establish the fluid velocities at the centers of the regular DEM grid. It also

performs the mapping of the force field back to the CFD code. Although the mapping operation is time-consuming, it has to be executed only once at the beginning.

The ACCI link stores and provides the required mapping coefficients as long as both codes (CFD and DEM) are running. The drag-force calculation is only performed by GPUs, where particle data are already available. The gas/solid fraction (which is in our code related to the DEM-cell) is only calculated by GPUs. Simultaneously with the drag force calculation, the coupling source term $\mathbf{S}_p$ for each DEM-cell is also obtained by GPUs together with the gas void fraction ε_f is transferred via ACCI. Furthermore, the transfer of the particle data from the GPUs to the CPUs memory is avoided. The transferred data amount is only dependent on the number of the DEM-cells and not on the number of particles. Considering that the number of DEM-cells usually does not exceed $O(10^6)$. The introduced coupling method is more efficient due to the minimized amount of the transfer data between CPUs and GPUs.

The DEM grid is regular and the velocity field data, as well as the inter-phase momentum source terms, are stored at the DEM grid's cell center. The fluid velocity used for the calculation of the drag force is interpolated to the particle position. The inter-phase momentum transfer source term is saved at the cell center of the DEM cell as well. An extrapolation scheme may be applied to distribute the drag force to all surrounding DEM cells, taking into account the distance between the particle and the cell centers of surrounding cells. However, a ratio of the particle diameter to DEM-cell size being too large can lead to numerical oscillations and instabilities [(Pepiot and Desjardins, 2012)]. Thus, this concept was not implemented and the particle growth was kept zero to maintain a constant particle diameter to DEM-cell size ratio throughout the simulation for bot cohesive and non-cohesive systems.

The gas phase modeling is based on locally volume-averaged quantities. Thus, the characteristic control volume V of the gas-phase numerical model must be at least an order of magnitude larger than the particle volume V_p, which is,

$V>10V_p$. Since the gas phase is resolved in three dimensions, the mesh size Δx must be chosen such that $\Delta x > (10\pi/6)^{1/3}d_p>1.74d_p$ for a valid coupled simulation when applying the point-particle approach.

The next limitation is associated with the time step, which must be selected such that the particle–particle interactions can be reproduced accurately. The time step should be sufficiently small to make sure that the contact lasts for a certain number of time steps to avoid problems concerning energy conservation due to the numerical integration. The contact time in the normal direction can be determined using expression according to [Deen et al. (2007)]:

$$\tau_{col,n} = \left(m_{AB}\frac{\pi^2+lne_{np\to p}^{\,2}}{k_n}\right)^{-1/2}$$

(29)

Analog to expression above, the time in the tangential direction is given by

$$\tau_{col,t} = \left(\frac{2}{7}m_{AB}\frac{\pi^2+lne_{tp\to p}^{\,2}}{k_t}\right)^{-1/2} \tag{30}$$

According to Deen et al. (2007), to maintain the energy balance the normal and tangential contact times should be the same, which leads to following relation between k_n and k_t:

$$\frac{k_t}{k_n} = \frac{2}{7}\frac{\pi^2+lne_{tp\to p}^{\,2}}{\pi^2+lne_{np\to p}^{\,2}} \tag{31}$$

The normal stiffness can be determined from Young's modulus and it usually yields a very high value, which requires very small time step and it is undesirable from the computation time point of view. However, in this work the

value of k_n was given by Van Buijtenen et al. (2011). The tangential stiffness k_t is calculated from Eq. (30).

4. Application of CFD-DEM Simulation

With the coupled CFD-DEM simulation a bottom spray Fluid Bed Coater with 200000particles was simulated for a process time of 30 sec. for the simulation 4CPUs and 1 GPU were used. The computational speed was about 3.5 sec/day.
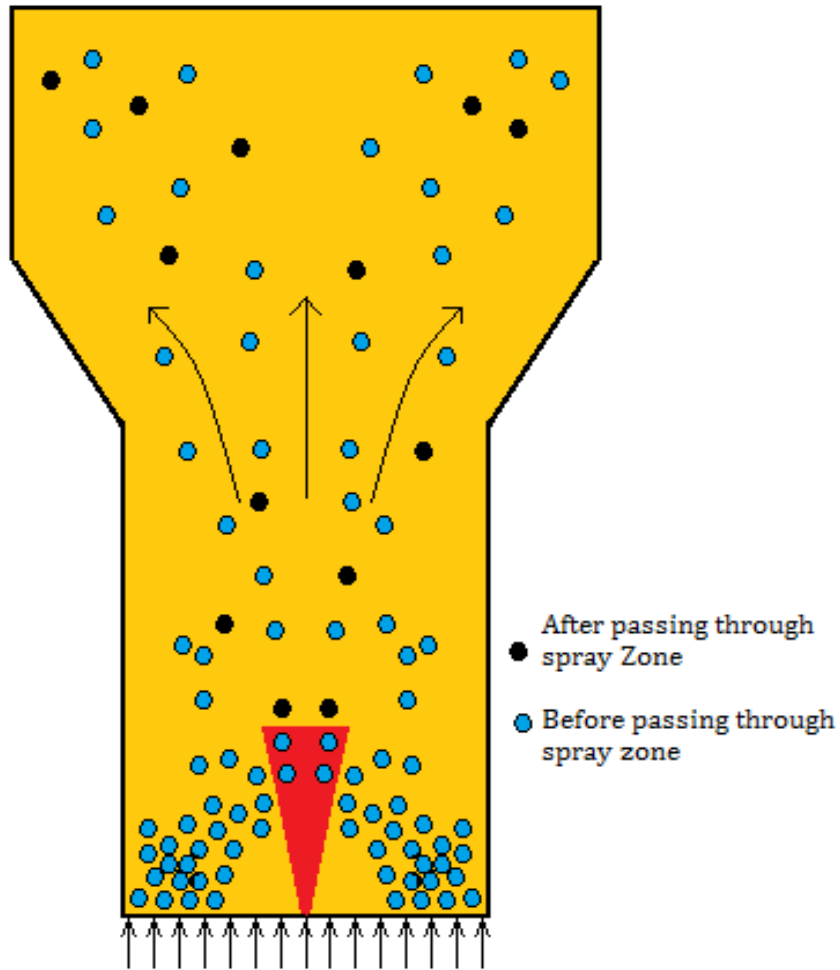
Fig. 3. Sketch of the bottom spray fluid bed coater.

The fluid bed consists of a cone in which the particles are fluidized due to incoming air entering through a distributing plate. The operating mode of the coater is shown in Fig. 3. The particles are fluidized through the incoming air and are coated in the spray zone, which is marked in red. Once the particles pass through the spray zone they change their color indicating they are coated.
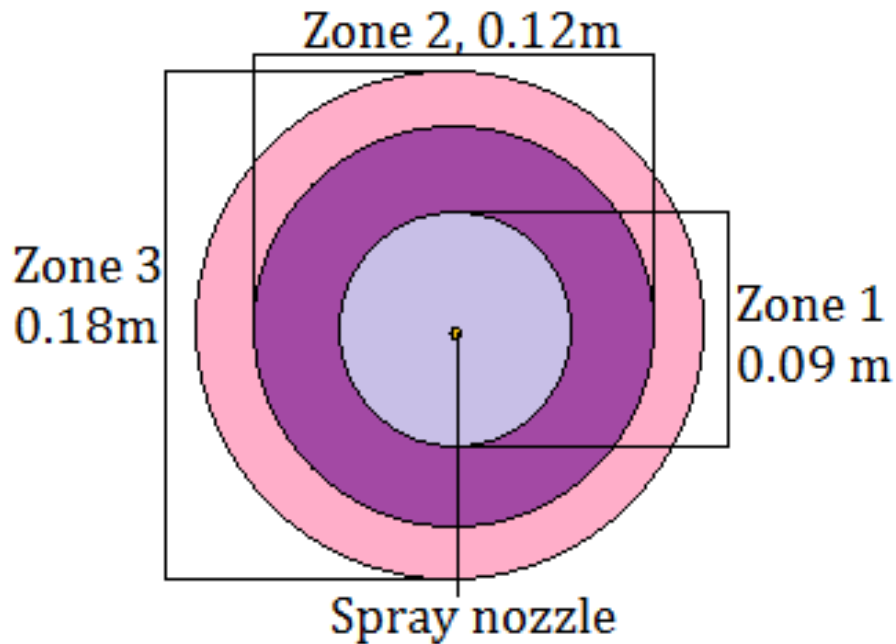
Fig. 4. Sketch of the distribution plate.

The distributing-plate at the bottom (Fig. 4) consists of three different regions with different air velocities. The region in the middle is the nozzle for spray inlet. Surrounding it is zone 1 which has the fluidization gas entering at higher velocity in this region. After the particles are sprayed they must be dried and also fluidized. So a higher gas velocity leads to a circulation of particles through the fluid bed and efficiently dries them. In the annulus (zone 2), the gas velocity is much lower than zone 1 and zone 3. Near the wall, zone 3, the gas velocity is slightly larger than in the annulus to avoid dead zones, where the particles are not moving. Due to the high air velocity under the spray zone the particles get fluidized, move up through the bed, and are transported to the wall and recirculate downwards.

Table 1: DEM simulation parameter and material

Property	Value	Unit

$N_{p,total}$	200 000	-
N_x	92	-
N_y	156	-
N_z	92	-
d_p	0.0018	M
P_p	1800	Kg/m^3
k_p	1000	N/m
$e_{n,p\rightarrow p}$	0.5	-
$e_{n,p\rightarrow w}$	0.8	-
$e_{t,p\rightarrow p}$	0.2	-
$e_{t,p\rightarrow w}$	0.2	-
DEM time step	10^{-5}	Sec
Particle mass	1.09	Kg
Spray rate	60	ml/min
Spray angle	20	Degree
Coating mass	0.027	Kg
t_{end}	30	sec

Table 1 lists the relevant simulation and material parameters used in the DEM-simulation. d_p is the diameter of a particle before it is coated and it remains constant throughout the simulation.

For analyzing the fluidization of cohesive and non-cohesive systems, four cases (case 1, case2, case 3 and case4) were considered. Table 2 lists the main simulation parameters used for the CFD-simulation for the above mentioned four cases.

Table 2. CFD simulation parameters

Property	Value	unit

Case 1	mass flow in zone 1	0.0099	kg/s
Non-Cohesive	mass flow in zone 2	0.0011	kg/s
	mass flow in zone 3	0.0094	kg/s
Case 2	mass flow in zone 1	0.009	kg/s
Cohesive	mass flow in zone 2	0.001	kg/s
	mass flow in zone 3	0.0085	kg/s
Case 3	mass flow in zone 1	0.0099	kg/s
Cohesive	mass flow in zone 2	0.0011	kg/s
	mass flow in zone 3	0.0094	kg/s
Case 4	mass flow in zone 1	0.0108	kg/s
Cohesive	mass flow in zone 2	0.0012	kg/s
	mass flow in zone 3	0.0103	kg/s
	Number of cells	186 764	-
	CFD time step	10^{-3}	Sec

In the presented case the DEM-code XPS uses a time step size of 10^{-5} sec which, in this simulation, ensures that contacts between particles last for a certain number of time steps to resolve particle collisions. This avoids problems concerning energy conservation. For the CFD-code a bigger time step size of 10^{-3} sec was used.

5. Results and Discussions

The study was conducted in three stages. Firstly the cohesive force model was tested. In second stage, a comparative approach between coating of particles with and without cohesive force models. In both the cases all the DEM-simulation parameters, CFD-simulation parameters and particle parameters were kept same (see Case 1 and Case 3 in Table 2). Though 30 sec of simulation does not represent the whole coating process, due to long simulation of 3.5 sec/day, the simulation end time was limited to

30 sec. In all stages the number of particles sprayed in every time step were monitored and a comparison was developed. Also the mean velocity of the system was monitored.

Fig. 5 shows a screenshot of Case 1 (see Table 1) simulation after a process time of 0.49 sec. The figure shows a cut through the YZ-plane of the simulation to allow a better insight into the process. Here the particles, which have not been coated, are grey. The ones, which are currently coated are green and those, which have already been coated are red.
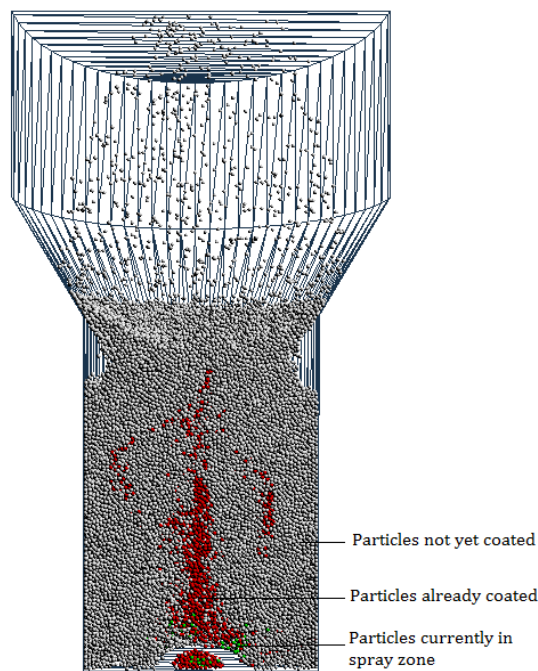
Fig. 5. Screenshot of Case 1 simulation after a process time of 0.49 sec.

5.1 Implementing the Cohesive Force model

An agglomerate should be defined as a group of particles connected by contact points which can exists even when forces other than cohesion and repulsion are removed. Accordingly, all particle-to-particle contact points were scanned and judged if a pair of particles in a particular contact point are separated after collision or not if no other forces exists based on the following criterion:

At contact point: $F_{rep,max} < F_{coh}$, (32)

Where $F_{rep,max}$ is the maximum repulsion force and F_{coh} is the maximum cohesion force by van der Waals force.

In numerical analysis an agglomerate is defined as a group of particles which are connected by preserved contacts. Fig. 6 shows the snapshots illustrating agglomerate formation of Case 3 simulation. Fig. 6(a) is for the case 1 of non-cohesive particles, where only those particles in collision are indicated. From Fig. 6, it can be confirmed that agglomerates size increase with longer simulation time.
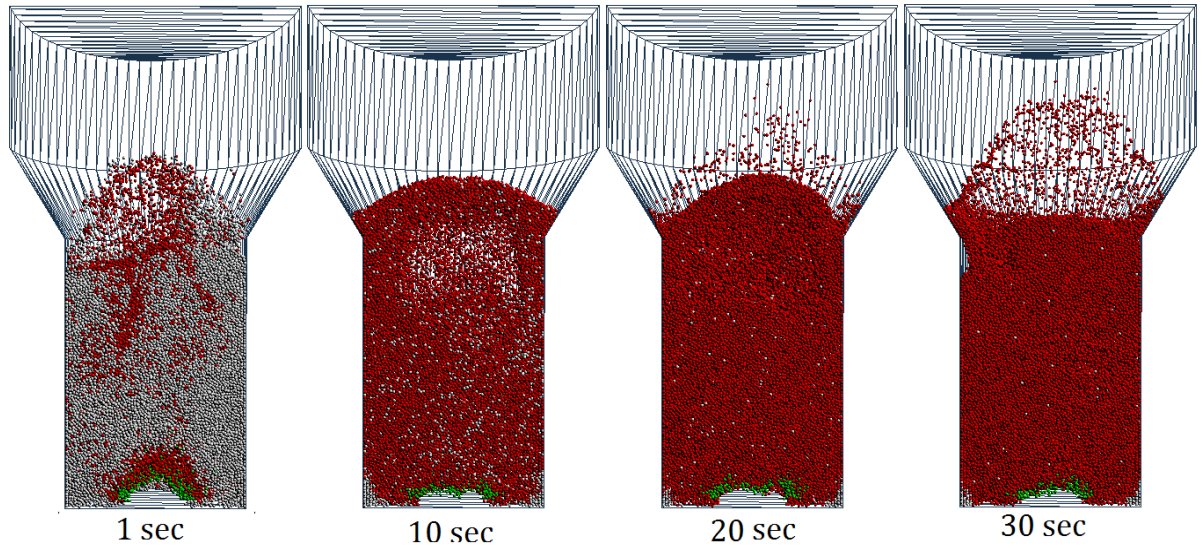
(a) Simulation with Case 1 parameters - Bed of Non-Cohesive particles
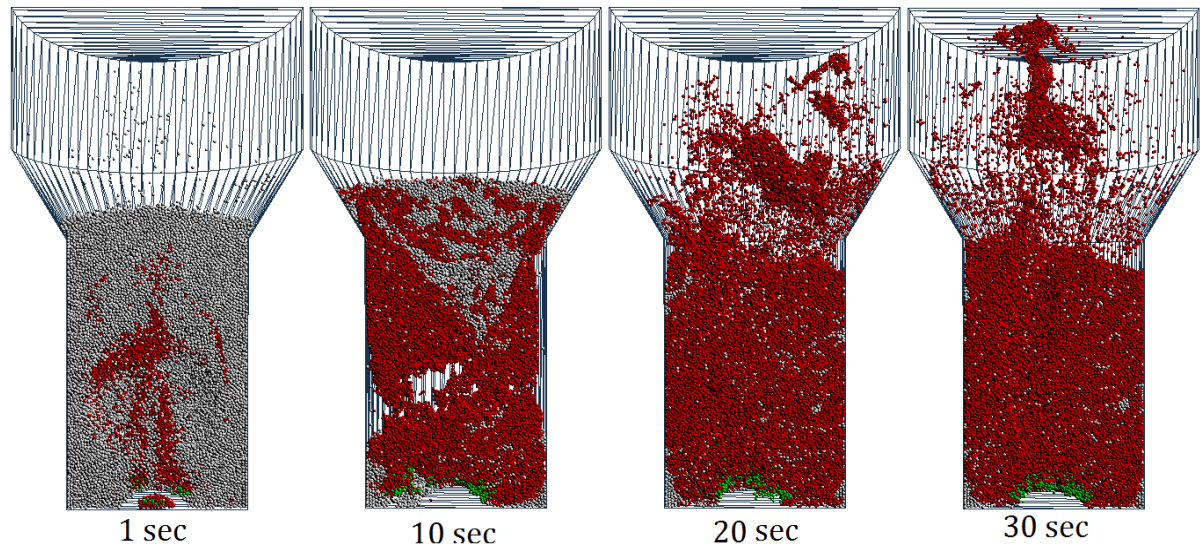
(b) Simulation with Case 3 parameters- Agglomerating fluidized bed

Fig. 6. Snapshots of behavior of (a) Non-cohesive particles and (b) agglomerating fluidized bed

Simulation with Case 3 parameters Fig. 7 shows the snapshots of velocity distribution and agglomerates in the bed. Particles which are connected to other particles by cohesion force can be observed in huge lumps.
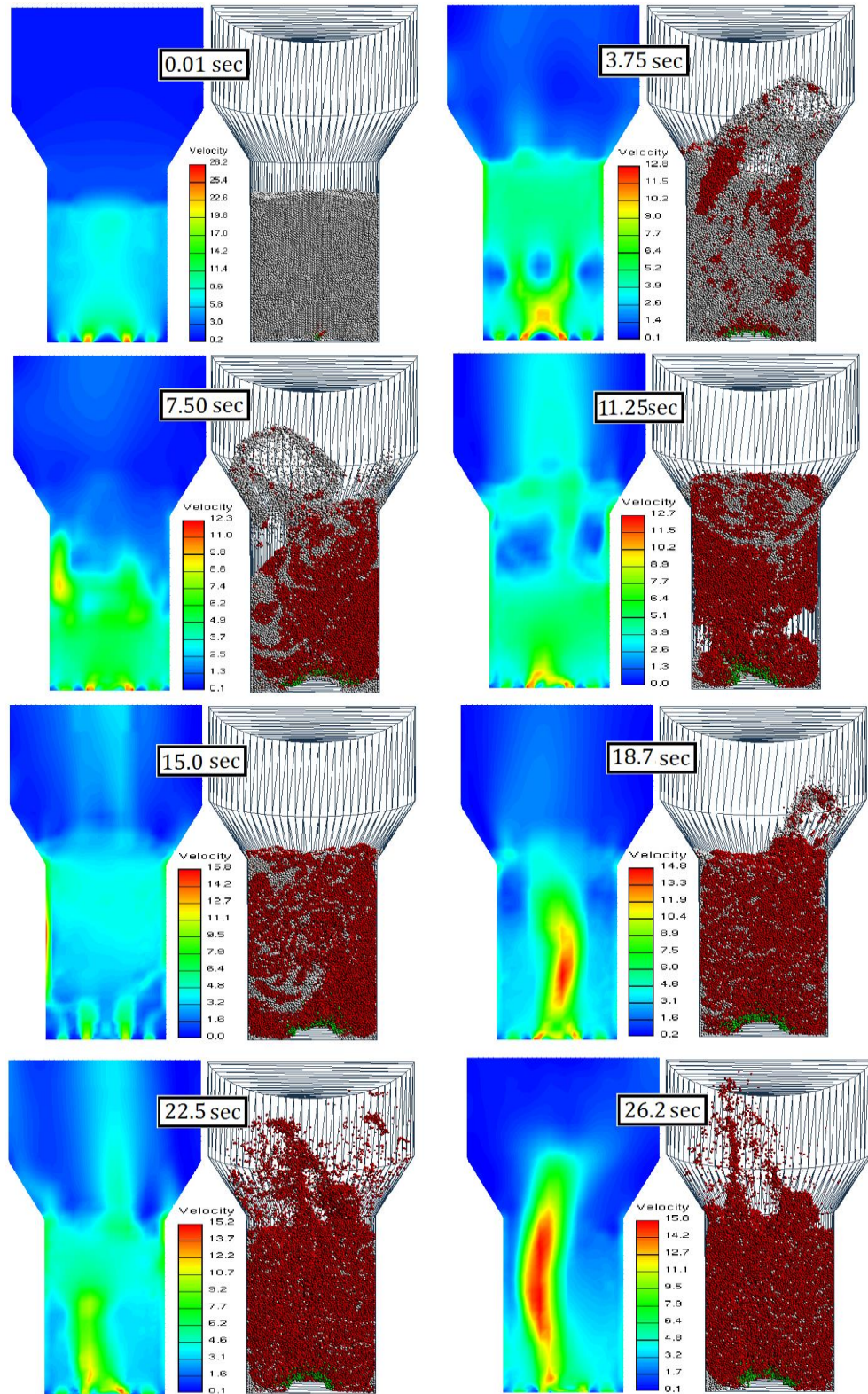
Fig. 7. Snapshots of velocity distribution (CFD-simulations) and corresponding particles (DEM-simulations) in the bed with Case 3 simulations.

The behavior of an agglomerate indicates that the agglomerate growth takes place below a rising bubble. On the other hand, the agglomerate breakage takes place above a bubble [Kenya kuwagi 2002]. This can be seen from Fig. 8 with Case 3 simulations. Fig. 9 shows particle growth and breakage with further magnification. In this case the simulation parameter taken are from Case 3 (Table 1).
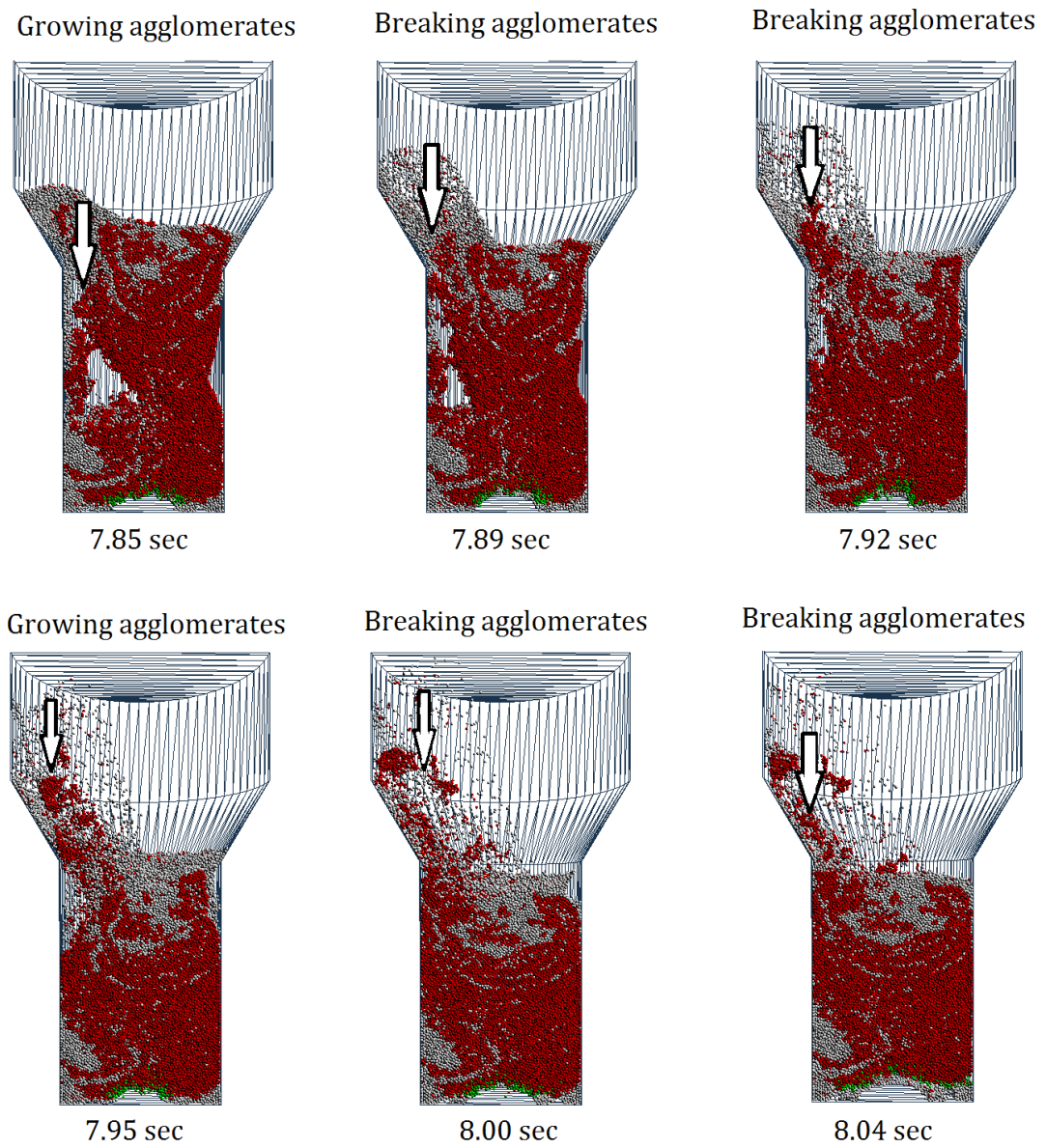
Fig. 8. Snapshots of agglomerates growth and breakage.

16.24 sec   16.26 sec   16.28 sec

16.30 sec   16.32 sec   16.34 sec
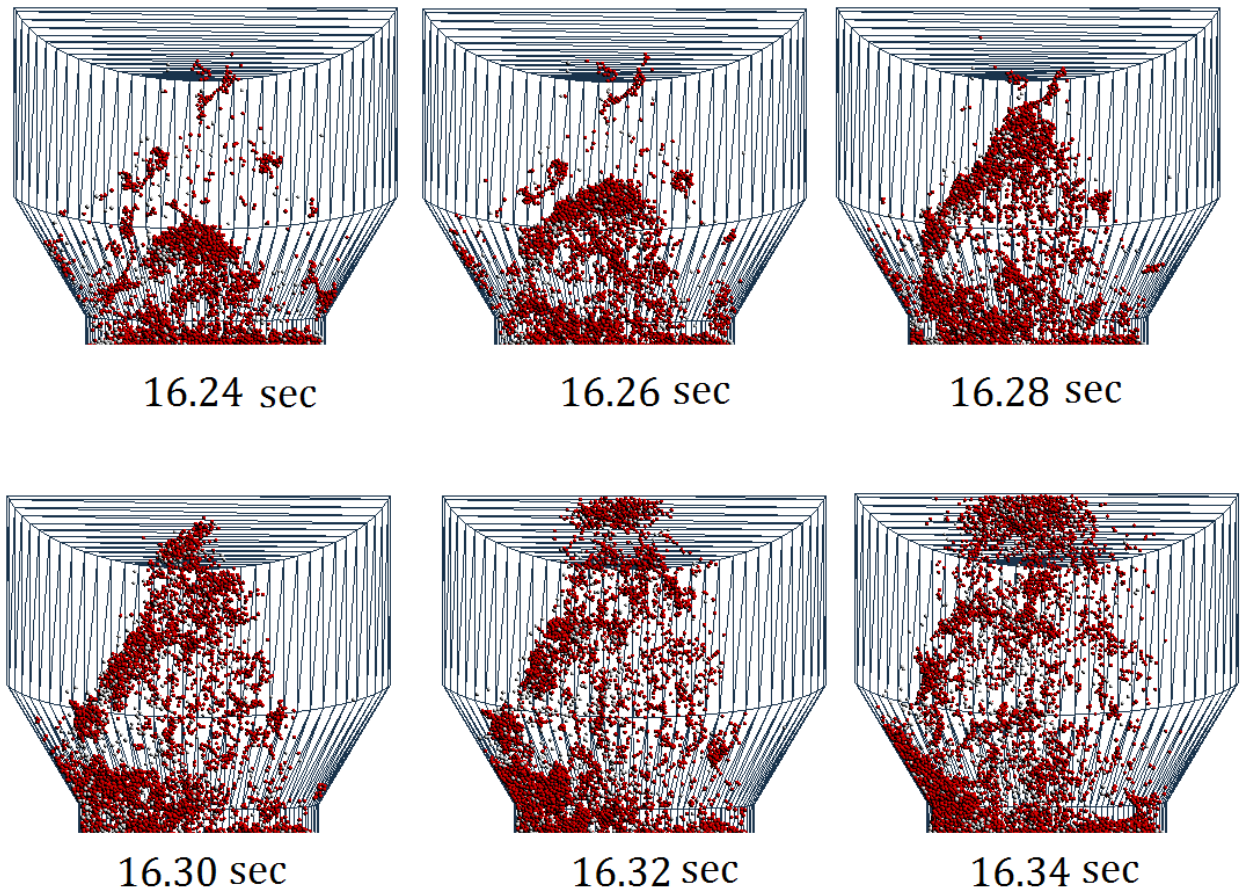
Fig. 9. Snapshots of growth and breakage with further magnification.

5.2 Comparison between Cohesive and Non-Cohesive systems

To understand the difference between the behavior of cohesive and non-cohesive number of particles sprayed and mean velocities were monitored in both cases. The simulations were done with parameters in Case 1 and Case 2. Both CFD-simulation parameters and DEM-simulation parameters are same. Fig. 10 shows snapshots of behavior of particles in both systems at same time steps. The snapshots (Fig. 10) clearly show that the system of non-cohesive particles were better fluidized. Also, the non-cohesive system is more homogeneous (well mixed).
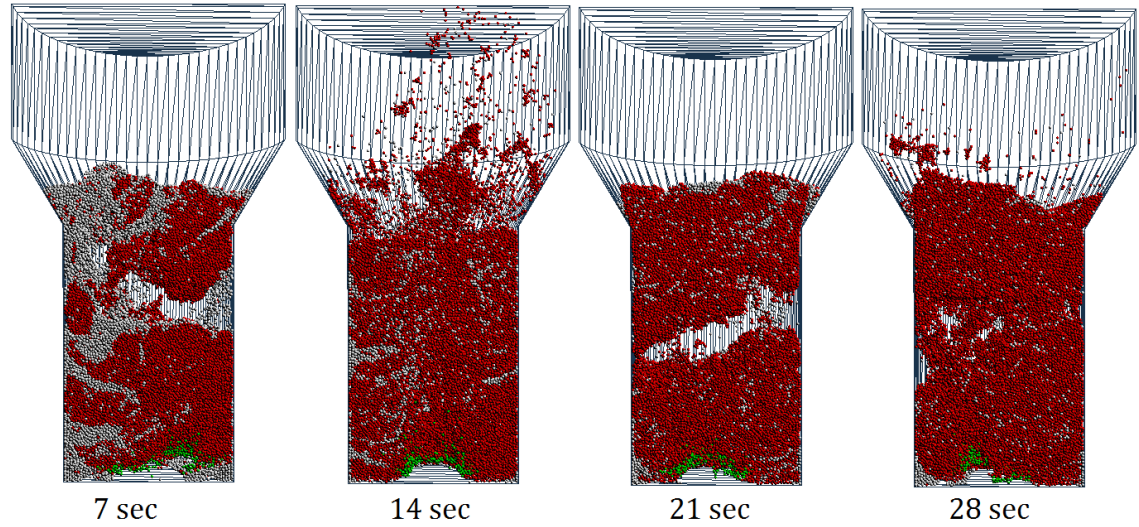
(a) Particle behavior in an agglomerating fluid bed with cohesive force model
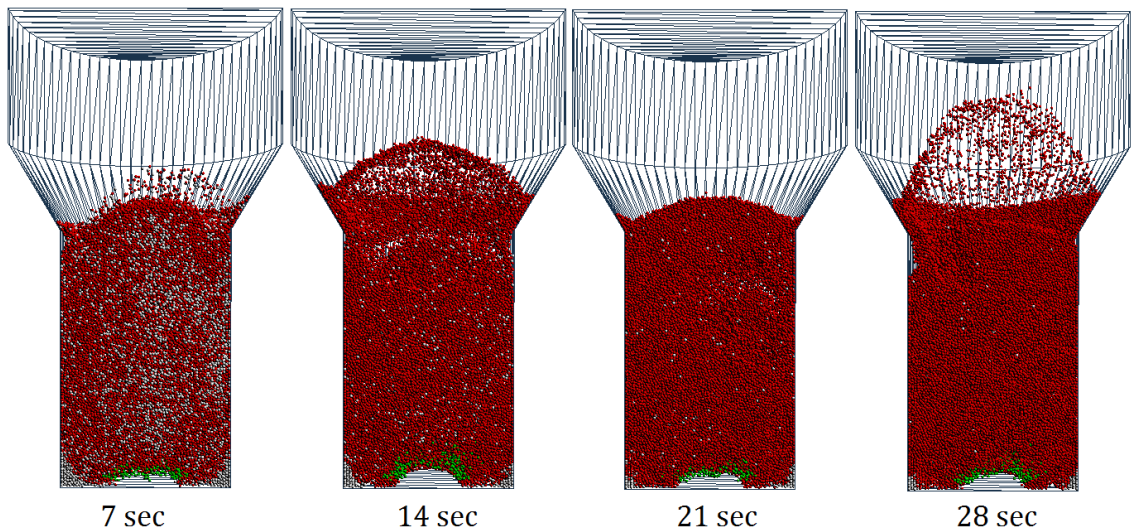

(b) Particle behavior in a fluid bed with no cohesive force model

Fig. 10. Snapshots comparing the behavior of fluidized particles in a (a) cohesive and (b) non-cohesive models.

Graph 1 shows the number of particles sprayed through the simulation time. It can be seen that more number of particles are sprayed in a non-cohesive system than compared to a cohesive system at any point of simulation. This is because of better fluidization and free flow of particles through the bed.

Number of particles sprayed over the simulation time
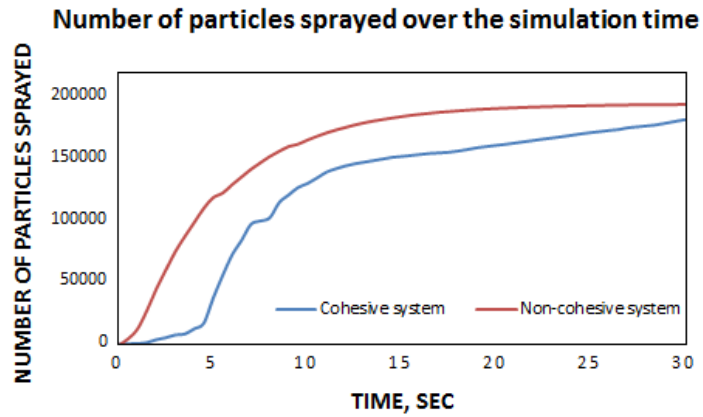
Graph 2. shows the mean velocities of both systems.

MEAN VELOCITY OF PARTICLES OVER THE SIMULATION TIME
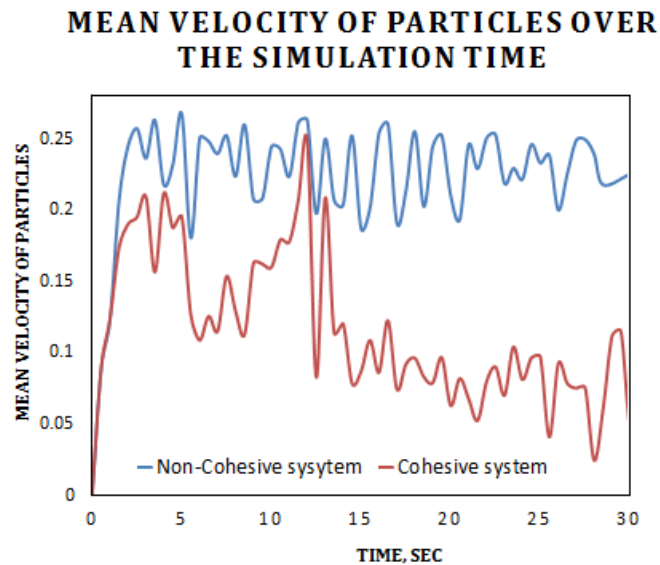
6. Conclusion

The agglomeration was observed with the new cohesive force model implemented. From the results of particles sprayed and velocity distribution it can be clearly seen that a non-cohesive powder are well suited for a fluidized bed. For the fluidization of cohesive powders more velocity is required.

7. Acknowledgments

8. Reference

[1] *Cole, G., Hogan, J., Aulton, M. E., & Twitchell, A. M. (2002). Pharmaceutical Coating Technology. (Graham Cole, Ed.). London: Taylor & Francis.*

[2] *Brock, D., Zeitler, J. A., Funke, A., Knop, K., & Kleinebudde, P. (2012). A comparison of quality control methods for active coating processes. Int J Pharm, 439(1-2), 289–95.*

[3] *Dubey, A., Boukouvala, F., Keyvan, G., Hsia, R., Saranteas, K., Brone, D., Muzzio, F. J. (2012). Improvement of tablet coating uniformity using a quality by Investigation of pharmaceutical tablet film coating processes using numerical simulations design approach. AAPS PharmSciTech, 13(1), 231–46.*

[4] *Mauritz, J. M. A., Morrisby, R. S., Hutton, R. S., Legge, C. H., & Kaminski, C. F. (2010). Imaging pharmaceutical tablets with optical coherence tomography. J Pharm Sci, 99(1), 385–91.*

[5] *Jajcevic, D., Siegmann, E., Radeke, C., & Khinast, J. G. (2013). Large-scale CFD–DEM simulations of fluidized granular systems. Chemical Engineering Science, 98, 298–310.*

[6] *Geldart, D., Types of gas fluidisation, Powder Technology 7, p. 285-292 (1973).*

[7] *D. Turki and N. Fatah. Behavior AND FLUIDIZATION OF THE COHESIVE POWDERS: AGGLOMERATES SIZES APPROACH. Brazilian Journal of Chemical Engineering, Vol. 25, No. 04, pp. 697 - 711 , October - December, 2008*

[8] *Radeke, C. A., Glasser, B. J., & Khinast, J. G. (2010). Large-scale powder mixer simulations using massively parallel GPU architectures. Chemical Engineering Science, 65(24), 6435–6442.*

[9] *Zhou, T. and Li, H., Estimation of agglomerate size for cohesive particles during fluidization, Powder Technology 101, p. 57-62 (1999)*

[10] *Lifshitz, E. M., The theory of molecular attractive forces between solids, Soviet Phys. JETP (Engl. Transl.) 2, p. 73-83 (1956).*

[11] Derjaguin, B.V. (1934). "Untersuchungen über die Reibung und Adhäsion, IV. Theorie des Anhaftens kleiner Teilchen" [Analysis of friction and adhesion, IV. The theory of the adhesion of small particles]. Kolloid Z. (in German) **69** (2): 155–164.

[12] Ketterhagen, W. R., am Ende, M. T., & Hancock, B. C. (2009b). Process modeling in the pharmaceutical industry using the discrete element method. Journal of pharmaceutical sciences, 98(2), 442–70

[13] Yamane, K., Sato, T., Tanaka, T., & Tsuji, Y. (1995). Computer simulation of tablet motion in coating drum. Pharmaceutical research, 12(9), 1264–8.

[14] Bedi, S., & Mirghasemi, A. A. (2011). Particle shape consideration in numerical simulation of assemblies of irregularly shaped particles. Particuology, 9(4), 387–397.